Ferrocenyl-Coupled N-Heterocyclic Carbene Complexes of Gold(I): a Successful Approach to Multinuclear Anticancer Drugs

Julienne K. Muenzner,[a] Bernhard Biersack,[a] Alexander Albrecht,[a] Tobias Rehm,[a] Ulrike Lacher,[a] Wolfgang Milius,[b] Angela Casini,[c,d] Jing-Jing Zhang,[e] Ingo Ott,[e] Viktor Brabec,[f,g] Olga Stuchlikova,[f,g] Ion C. Andronache,[h] Leonard Kaps,[i] Detlef Schuppan,[i,j] and Rainer Schobert*[a]

Abstract: Four gold(I) carbene complexes featuring 4-ferrocenyl substituted imidazol-2-ylidene ligands were investigated for antiproliferative and antivascular properties. They were active against a panel of seven cancer cell lines, including multidrug-resistant ones, with low micromolar or nanomolar IC_{50} (72 h) values, according to their lipophilicity and cellular uptake. The delocalised lipophilic cationic complexes **8** and **10** acted by increasing the reactive oxygen species in two ways: via a genuine ferrocene effect and by inhibiting the thioredoxin reductase. Both complexes gave rise to a reorganization of the F-actin cytoskeleton in endothelial and melanoma cells, associated with a G1 phase cell cycle arrest and a retarded cell migration. They proved antiangiogenic in tube formation assays with endothelial cells and vascular-disruptive on real blood vessels in the chorioallantoic membrane of chicken eggs. Biscarbene complex **10** was also tolerated well by mice where it led to a volume reduction of xenograft tumors by up to 80%.

[a] Dr. J.K. Münzner, Dr. B. Biersack, A. Albrecht, T. Rehm, Dr. U. Lacher
Organic Chemistry Laboratory
University Bayreuth
Universitätsstraße 30, 95447 Bayreuth (Germany)
E-mail: Rainer.Schobert@uni-bayreuth.de
[b] Dr. W. Milius
Lehrstuhl für Anorganische Chemie I
Universität Bayreuth
Universitätsstraße 30, 95447 Bayreuth (Germany)
[c] Prof. Dr. A. Casini
Department of Pharmacokinetics, Toxicology, and Targeting
University of Groningen
Antonius Deusinglaan 1, 9713 Groningen (The Netherlands)
[d] School of Chemistry, Cardiff University
Main Building, CF10 3AT Cardiff (UK)
[e] Dr. J.-J. Zhang, Prof. Dr. I. Ott
Medicinal and Pharmaceutical Chemistry
Technische Universität Braunschweig
Beethovenstraße 55, 38106 Braunschweig (Germany)
[f] Prof. Dr. V. Brabec, O. Stuchlikova
Institute of Biophysics, Academy of Sciences of the Czech Republic
Kralovopolska 135, CZ-61265 Brno (Czech Republic)
[g] Dept. of Biophysics, Faculty of Science
Palacky University
Listopadu 12, CZ-77146 Olomouc (Czech Republic)
[h] Dr. I. C. Andronache
Research Centre for Integrated Analysis and Territorial Management, University of Bucharest
1 Nicolae Balcescu bvd., district 1, 010055 Bucharest (Romania)
[i] L. Kaps, Prof. Dr. Dr. D. Schuppan
Institute of Translational Immunology
University Medical Center of the Johannes Gutenberg University
Langenbeckstraße 1, 55131 Mainz (Germany)
[j] Prof. Dr. Dr. D. Schuppan
Division of Gastroenterology, Beth Israel Deaconess Medical Center
Harvard Medical School, Boston (US)
Supporting information for this article is given via a link at the end of the document.

Introduction

A common strategy to improve the impact of metallodrugs is the optimization of their pharmacokinetic and pharmacodynamic properties.[1,2] A less frequent approach uses the decoration of bioactive metal fragments with ligands or shuttle groups that show some bioactivity or functionality of their own. In felicitous cases pleiotropic drugs result that not only retain the individual properties of metal and ligand but also exhibit some new effects.[3–6] *N*-heterocyclic carbene (NHC) ligands are poor leaving groups and thus lend themselves ideally to the permanent introduction of modulatory substituents at their heterocycle.[3,6] Previously, we reported on gold(I) mono- and biscarbene complexes (**1**, **2**) with imidazole ligands that had been modeled on the natural antivascular agent combretastatin A-4 (CA-4) (Figure1).[7–9] They proved highly cytotoxic and efficacious against cancer cell lines of various entities with IC_{50} values in the low micromolar or even submicromolar range. Despite their different molecular mechanism of action when compared to CA-4, they also retained a significant antivascular activity both *in vitro* and *in vivo*.

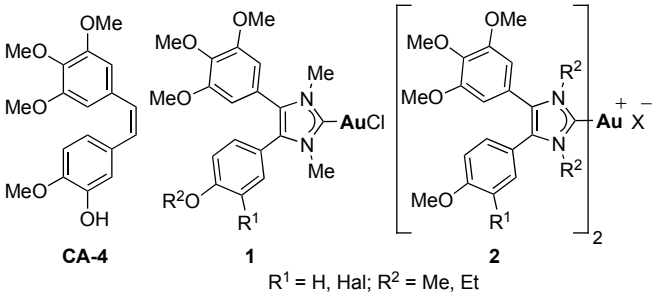

Figure 1. The natural vascular-disruptive agent combretastatin A-4 (CA-4) and its analogous gold(I) NHC complexes **1** and **2**.

Since gold NHC complexes had been reported to interfere with the redox machinery of cells, e.g., the mitochondria or specific antioxidative enzymes such as thioredoxin reductase (TrxR),[3,5,6] we intended to attach an electronically coupled, redox-active ferrocenyl residue to the NHC ligand of gold(I) complexes. The concept of enhancing the activity or selectivity of anticancer metallodrugs by introduction of further metal centers is not new.[10–13] Ferrocene is known to activate lymphocytes and to exert distinct antitumor effects which are associated with the production and regulation of reactive oxygen species (ROS) and the oxidation of Ras proteins at cysteine sites.[14] A host of antitumoral ferrocene derivatives have been published, including

conjugates with peptides, benzotriazoles, nucleobases, estrogen receptor modulators, and fungal cytotoxins like illudin M.[15–19] There are also reports on gold complexes conjugated to ferrocene with distinct anticancer activities against various cancer cell lines.[11,20] In the present paper, we report on the synthesis and structure-dependent anticancer properties *in vitro* and *in vivo* of new carbene complexes of gold(I) featuring ferrocenyl-coupled imidazol-2-ylidene ligands.

Results and Discussion

Chemistry

The *N*-alkyl-5-ferrocenyl-4-phenyl-imidazoles **4** were obtained via a Van-Leusen imidazole synthesis starting from ferrocenyl carboxaldehyde and the TosMIC reagent **3** (Scheme 1). Alkylation of complexes **4** with iodomethane or iodoethane afforded the corresponding imidazolium salts **5**, which were treated with silver(I) oxide to give the silver(I) carbene complexes **6**. Their transmetallation with chlorido(dimethylsulfide)gold(I) gave the chlorido(NHC)gold(I) complexes **7**. The cationic phosphano gold complex **8** was obtained from the reaction of **7b** with PPh_3 and $NaBF_4$.[21]

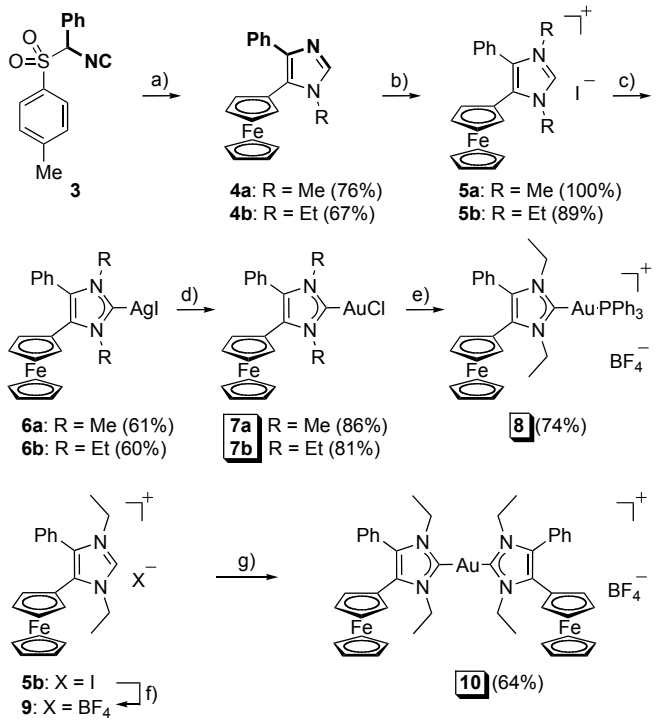

Scheme 1. Syntheses of gold(I) NHC complexes **7**, **8**, and **10**. Reagents and conditions: a) ferrocenyl carboxaldehyde, 33% $MeNH_2$/EtOH or 2M $EtNH_2$/THF, AcOH, EtOH, reflux, 2 h, then **3**, K_2CO_3, EtOH, reflux, 3 h; b) MeI or EtI, MeCN, 80 °C, 16 h; c) Ag_2O, CH_2Cl_2, r.t., 16 h; d) $Cl(Me_2S)Au$, CH_2Cl_2, r.t., 16 h; e) **7b**, $NaBF_4$, PPh_3, acetone, r.t., 1 h; f) $NaBF_4$, acetone, r.t., 16 h, 100%; g) Ag_2O, CH_2Cl_2, r.t., 5 h, then $Cl(Me_2S)Au$ (0.5 equiv.), CH_2Cl_2, r.t., 16 h.

The cationic biscarbene complex **10** was prepared from imidazolium iodide **5b** which had its counter anion substituted for BF_4 to give complex **9**. This was converted with Ag_2O to the corresponding silver carbene complex which was not isolated but transmetallated with 0.5 equivalents of $Cl(Me_2S)Au$ to afford complex **10** (Scheme 1, bottom row). Crystals of complex **10** suitable for X-ray diffraction analyses were grown by slow infusion of ether into a saturated CH_2Cl_2 solution at 4 °C (Figure 2). The cyclic voltammograms of the new complexes showed an anodic shift of the redox potential $E_{1/2}$ relative to ferrocene, e.g. by 145 mV in the case of neutral **7b** (*cf.* Supporting Information).

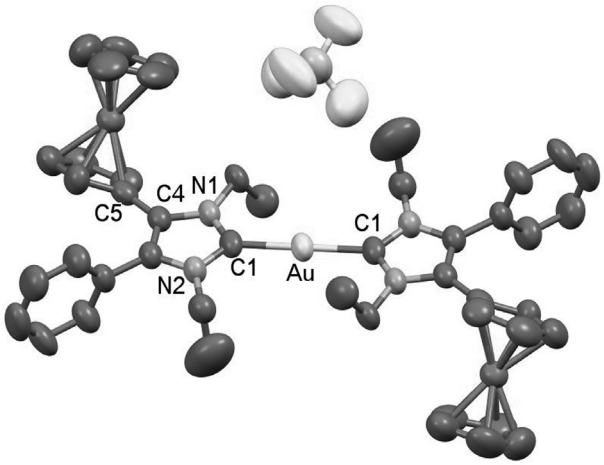

Figure 2. Molecular structure of complex **10** as thermal ellipsoid representation at 50% probability level (H atoms omitted). Selected bond lengths [Å] and angles [°]: Au-C1 2.02, C1-N1 1.35(1), N1-C4 1.38(1), C4-C5 1.44(1), C5-Fe 2.092(8), C1-Au-C1 180.0, Au-C1-N1 127.0, N1-C1-N2 105.8(7), C5-C4-N1 126.8(8).

Antiproliferative activity in vitro

The effect of complexes **7**, **8**, and **10** on the growth of cancer cells was evaluated in proliferation assays using 3-(4,5-dimethylthiazol-2-yl)-2,5-diphenyltetrazolium bromide (MTT) that is reduced to a violet formazan in viable cells.[22] To assess potential selectivities for cancer over non-malignant cells, CCD18-Co colorectal myofibroblasts were included (Table 1). The *N*-methylated monocarbene complex **7a** was antiproliferative with IC_{50} values mostly in the lower micromolar range (IC_{50} (72 h) = ca. 7–20 μM), while its *N*-ethyl analog **7b** was significantly more active (IC_{50} (72 h) = ca. 0.2–4 μM). Moreover, we found that replacing the chlorido ligand by a triphenylphosphane or a second NHC ligand, as in the cationic complexes **8** and **10**, further enhanced the antiproliferative effect, giving rise to IC_{50} values in the lower submicromolar range with complex **10** being slightly more active than complex **8**. This trend of increasing cytotoxicities when substituting a chlorido for a phosphane or NHC ligand has previously been observed for NHC gold(I) complexes of the benzimidazol-2-ylidene type by Rubbiani *et al.*[23] Interestingly, all complexes **7**, **8**, and **10** were active also against multidrug-resistant tumor cell lines such as HT-29 colon,[24,25] MCF-7/Topo breast,[26,27] and – with the exception of complex **7a** – KB-V1/Vbl cervix carcinomas. Pretreatment of KB-V1/Vbl cells which overexpress P-glycoprotein

1[28-30] with verapamil, an inhibitor of this efflux transporter, for 24 h improved the effect of all complexes by a factor of 4 to 35. This suggests that they are themselves substrates of P-gp, like the CA-4 derived biscarbene complexes **2**.[9] The complexes **7**, **8**, and **10** also strongly inhibited the growth of human umbilical vein endothelial cells (HUVEC), which is a hint at a potential antivascular activity. In contrast, the non-malignant CCD18-Co fibroblasts were affected only at higher complex concentrations.

Table 1. Inhibitory concentrations[a] IC_{50} [μM] of complexes **7**, **8**, and **10** when applied to human cancer cells and non-malignant cells.

Cell line[b]	7a	7b	8	10
518A2	11.3 ± 0.3	1.3 ± 0.1	0.20 ± 0.03	0.19 ± 0.02
Panc-1	6.7 ± 0.3	0.62 ± 0.01	0.14 ± 0.02	0.09 ± 0.00
MCF-7/Topo	7.1 ± 0.1	0.71 ± 0.02	0.60 ± 0.01	0.11 ± 0.00
KB-V1/Vbl	> 50	13.3 ± 0.1	1.6 ± 0.4	1.5 ± 0.1
KB-V1/Vbl +verapamil	2.0 ± 0.6	0.38 ± 0.12	0.40 ± 0.08	0.11 ± 0.01
HCT-116	11.1 ± 0.3	0.21 ± 0.08	0.09 ± 0.01	0.06 ± 0.00
HT-29	10.8 ± 0.4	0.30 ± 0.08	0.16 ± 0.02	0.13 ± 0.01
DLD-1	19.5 ± 1.0	4.2 ± 1.4	1.2 ± 0.5	0.30 ± 0.11
HUVEC	12.0 ± 1.5	0.68 ± 0.07	0.77 ± 0.17	0.26 ± 0.04
CCD-18Co	> 50	15.0 ± 0.9	8.9 ± 0.3	2.8 ± 0.1

[a] Values are derived from dose-response curves obtained by measuring the percentage of viable cells relative to untreated controls after 72 h of incubation using MTT assays. Values represent means of four experiments ± standard deviations. [b] Human cancer cell lines: 518A2 melanoma, Panc-1 pancreatic ductular adenocarcinoma, MCF-7/Topo breast adenocarcinoma, KB-V1/Vbl cervix carcinoma (optionally pretreated with 24 μM verapamil for 24 h), HCT-116 colon carcinoma, HT-29 and DLD-1 colorectal adenocarcinoma; human non-malignant cells: HUVEC primary human umbilical vein endothelial cells and CCD-18Co human colon fibroblasts.

Cellular accumulation and lipophilicity

The activity of drugs depends on their intracellular accumulation. The uptake of complexes **7**, **8**, and **10** by HCT-116 cells that had been exposed to 0.5 μM concentrations of the compounds for 24 h, was measured by ICP-MS analysis of their iron content (Table 2). Additionally, the coefficient log P for their partition between 1-octanol and water was determined in order to identify correlations between lipophilicity, cellular uptake and cytotoxicity.[31,32] They displayed a largely hydrophilic character with negative log P values that correlate with their respective cellular accumulation. The most hydrophilic complex **7a** showed the least uptake. Its more lipophilic *N*-ethyl analog **7b** was taken up to a greater extent. The cytotoxicities of the complexes **7** tie in nicely with their lipophilicities and accumulations. Complex **7b** is active in HCT-116 cells with an IC_{50} value about 50 times lower than that of complex **7a**. The cationic phosphane complex **10** has a log P value near 0 and thus a greater lipophilicity than the neutral complexes **7**. Consequently, it also showed the greatest accumulation in HCT-116 cells which fits in with its high cytotoxicity against this cancer cell line.

Table 2. Cellular iron uptake from complexes **7**, **8**, and **10** in HCT-116 colon carcinoma cells and their log P (1-octanol/water) values. Cells were exposed to the test compounds (0.5 μM) for 24 h before analyzing the metal content. The log P values of the complexes were determined by the shake flask method. The results are expressed as means ± SD of three independent samples for each experiment.

	7a	7b	8	10
ng Fe / 10^6 cells	3.06 ± 0.06	4.17 ± 0.04	3.15 ± 0.05	18.9 ± 1.6
log P	–1.71 ± 0.05	–0.07 ± 0.01	–1.30 ± 0.02	0.06 ± 0.00

Effects on the cytoskeletal organization

Like the CA-4 derived complexes **1** and **2**,[7–9] the new ferrocenyl complexes did not interfere with the polymerization of tubulin or with the organization of microtubules in cells, but induced a distinct reorganization of the actin cytoskeleton in both 518A2 melanoma cells and non-malignant HUVEC. For instance, when we visualized microtubules (not shown) and filamentous actin (F-actin) in these cells after treatment with 500 nM of **8** or 250 nM of **10**, we saw changes only in the organization of the latter (Figure 3). Both complexes led to the formation of sheaves of parallel actin fibers running across the entire cell bodies, in contrast to the cortical networks of actin observed in untreated control cells. The stress fiber formation was more pronounced in HUVEC than in the tumor cells, and more for complex **10** than for complex **8**.

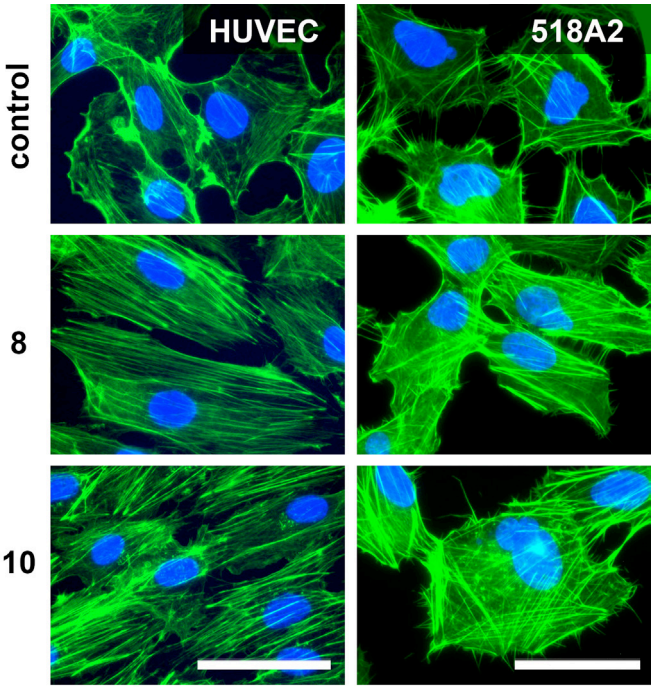

Figure 3. Effects on the organization of F-actin in human vascular endothelial (HUVEC) and 518A2 melanoma cells. Both cell lines were treated with 500 nM of **8**, 250 nM of **10**, or DMF as vehicle control for 24 h. Scale bar - 50 μm.

Effects on tumor cell cycle and migration

The effects of complexes **8** and **10** on the cell cycle progression of 518A2 melanoma cells were analyzed by propidium iodide staining and flow cytometry (Figure 4A). Both complexes induced a significant accumulation of cells in the G1 phase, with complex **10** again being slightly more effective. The fractions of cells in S and G2/M phase were distinctly reduced while the sub-G1 population of apoptotic cells rose slightly for the applied concentrations of complexes **8** (500 nM) and **10** (250 nM).

Both, the reduced dynamics of the actin cytoskeleton and the marked G1 phase arrest diminished the motility and thus invasiveness of the melanoma cells.[33,34] In so-called wound healing assays the complexes **8** and **10** reduced their ability to close artificial wounds, i.e., scratches in cell monolayers when compared to untreated cells. While treatment of 518A2 cells with 500 nM of complex **8** for 48 h reduced the wound healing to ca. 70%, the biscarbene complex **10** was a more potent inhibitor of cell migration, reducing the wound healing to ca. 40% when applied at the same concentration (Figure 4B).

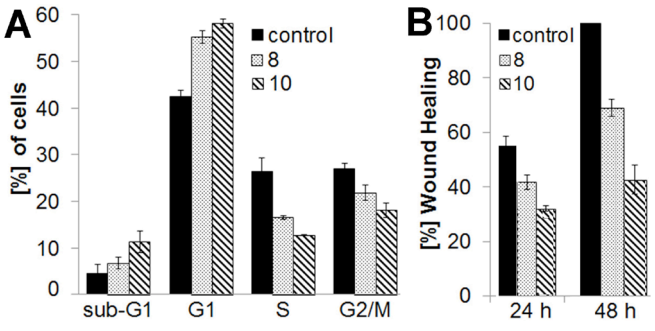

Figure 4. A) Fractions of 518A2 melanoma cells in G1, S, and G2/M phase of the cell cycle, and apoptotic cells (sub-G1 population) upon treatment with 500 nM of **8**, 250 nM of **10**, or vehicle for 24 h as obtained by flow cytometry after DNA staining with propidium iodide. Values represent means ± SD of three independent experiments. B) Inhibitory effects of complexes **8** and **10** (500 nM) on the migration of 518A2 melanoma cells in wound healing assays. Values represent means ± SD of three experiments.

Interference with the tumor cell redox poise

The thioredoxin reductase (TrxR) is involved in maintaining the intracellular redox homeostasis and plays an important role in the regulation of cell proliferation and survival.[36,37] Its inhibition leads to an increase of reactive oxygen species (ROS) in cells, to an interference with mitochondrial functions, and eventually to apoptosis. Since TrxR had already been identified as an important target of gold(I) NHC complexes[3,5,6,38,39] we analyzed the cationic complexes **8** and **10** for a potential inhibition of isolated TrxR *in vitro*. The phosphane complex **8** proved a potent TrxR inhibitor with an EC_{50} = 0.6 ± 0.1 µM, while the biscarbene complex **10** was slightly less effective with an EC_{50} = 1.5 ± 0.2 µM. A possible explanation for this difference is that triphenylphosphane is a better leaving group than an NHC ligand. This allows a faster binding interaction of the gold center of complex **8** with the selenocysteine residue in the active site of the TrxR. Recently, Rubbiani *et al*. reported a similar gradation of the TrxR inhibiting effects of phosphane *vs.* NHC substituted benzimidazolylidene gold(I) complexes.[23,38] The different potential of complexes **7b**, **8**, and **10** to inhibit the seleno-enzyme TrxR was also assessed by a model reaction with *in situ* generated seleno-L-cysteine and MS analytics of the resulting adducts as previously described.[40,41] We found that complexes **7b** and **8** readily formed mono selenol adducts with substitution of the chloro or phosphane ligands, respectively, while the biscarbene complex **10** did not (*cf.* Supporting Information).

Additionally, we tested them for inhibition of purified poly(ADP-ribose) polymerase 1 (PARP-1), an enzyme that plays an important role during the initiation of DNA repair and in drug resistance mechanisms of cancer cells. PARP-1 has also been identified, recently, as a target for gold complexes as well as for heteronuclear iron-gold complexes.[11,42,43] Complex **10** was a more effective inhibitor of PARP-1 (EC_{50} = 1.0 ± 0.4 µM) than complex **8** (EC_{50} = 2.0 ± 0.3 µM). Previously, Lease *et al.* reported a trinuclear Fe-Au(III) complex that also inhibited PARP-1 with an EC_{50} of ca. 1 µM.[11] It should be noted, though, that other Au(I) and Au(III) complexes with N-donor and phosphane ligands are known that inhibit PARP-1 with EC_{50} values in the nanomolar range.[42,43]

Reactive oxygen species (ROS) are associated with the mode of action of ferrocene derivatives. There are numerous studies of the correlation between ROS production and antiproliferative effects of ferrocenes, including heteronuclear ferrocene–gold complexes.[14,20,44] The effect of complexes **8** and **10** on the ROS levels in 518A2 melanoma cells was now investigated by the nitroblue tetrazolium chloride (NBT) test (Figure 5A). When applied at lower concentrations, only complex **10** led to an increase of ROS. At a concentration of 500 nM it caused a 1.6 times higher level of ROS when compared with untreated control cells, while complex **8** had virtually no effect at this concentration. However, at the highest applied concentration of 1 µM both complexes raised the ROS levels equally to ca. 180 % relative to controls. There seem to be at least two ROS increasing effects: a genuine ferrocene effect, which explains the higher ROS levels initiated by the bisferrocenyl complex **10** at lower concentrations, and the rise of ROS levels brought about via TrxR inhibition[38,45,46] which is more pronounced for the monoferrocenyl complex **8** and which overrides the stronger ferrocene effect by complex **10** at higher concentrations.

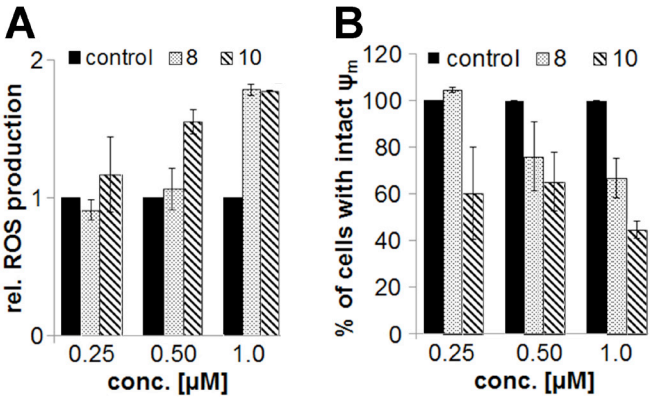

Figure 5. A) ROS levels in 518A2 melanoma cells as determined by NBT assays. Cells were treated with 250 nM, 500 nM, or 1 µM of complexes **8** and **10** or respective amounts of DMF (controls) for 24 h. Values represent means

± SD of two independent experiments in triplicate. B) Effects on the mitochondrial membrane potential in 518A2 melanoma cells as observed in JC-1 assays with cells treated as above. Values represent means ± SD of two independent experiments in triplicate.

The mitochondrial membrane potential $\Delta\psi_m$ is known to be affected by the inhibition of TrxR by gold(I) complexes.[45–48] Both complexes **8** and **10** are delocalized lipophilic cations (DLC), which are known to accumulate in mitochondria, disturb essential functions of these, and lead to the loss of $\Delta\psi_m$, eventually inducing the intrinsic pathway of apoptosis.[49–51] The effects of complexes **8** and **10** on the $\Delta\psi_m$ in 518A2 melanoma cells were evaluated by a JC-1 assay (Figure 5B). Both complexes initiated a concentration-dependent reduction in the fraction of cells with an intact $\Delta\psi_m$. Despite its less pronounced TrxR inhibition the biscarbene complex **10**, when applied at 1 µM, reduced the fraction of cells with unaltered $\Delta\psi_m$ to ca. 45%, and thus more strongly than complex **8** which left ca. 65% of mitochondria with intact $\Delta\psi_m$. A possible explanation lies in the higher lipophilicity of complex **10** which facilitates its uptake into mitochondria.[52]

Antivascular effects

Tube formation assay: To assess the antiangiogenic activity of complexes **8** and **10** we performed *in vitro* tube formation assays which are based on the ability of vascular endothelial cells to form interconnected networks of capillary-like structures when grown on an extracellular membrane matrix support such as matrigel.[53] For this, HUVEC were seeded on matrigel, treated with various concentrations of the test compounds and the effects on the formation of tubular networks were documented after 24 h of incubation. Figure 6 shows the results. While control cells had built up highly organized networks of capillary-like structures, both complexes **8** and **10** strongly impaired the formation of such tubular structures when applied at concentrations as low as 100 nM.

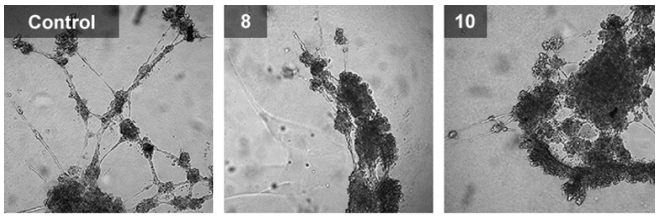

Figure 6. Inhibitory effects of complexes **8** and **10** (each 100 nM) on the formation of organized tubular networks by HUVEC seeded on matrigel after 24 h of incubation.

The chorioallantoic membrane (CAM) of fertilized chicken eggs is highly vascularized and serves as the respiratory system.[54,55] It can be used as a simple *in vivo* model system to study the antiangiogenic or vascular-disruptive effects of new drug candidates.[9,54–56] Figure 7 depicts the antivascular effects of complexes **8** and **10** in comparison to the normal development of blood vessels in the CAM. After 6 h of incubation complex **8** had destroyed nearly all smaller capillaries while complex **10** had affected even bigger vessels and had induced hemorrhages. These effects were quantified by a vessel area analysis based on a fractal analysis as described previously.[9,57] The area of blood vessels was decreased to 47 ± 6% by complex **8**, and to 27 ± 1% by complex **10**. After 24 h of incubation with complex **8** the vasculature within the treated area had recovered and the sprouting of new blood vessels was detected. In contrast, treatment with complex **10** for 24 h led to a further destruction of the vasculature.

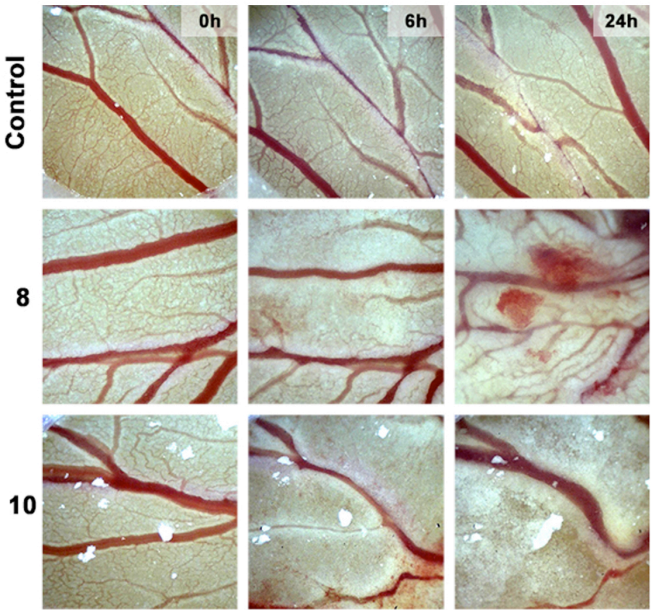

Figure 7. Antivascular effects of complexes **8** and **10** on the chorioallantoic membrane of fertilized chicken eggs. Images were taken 6 h and 24 h after application of the test compounds (2.5 nmol) on day 7 post fertilization and are representative of at least three independent assays.

In vivo mouse xenograft model

The antitumoral activity of biscarbene complex **10** was further assessed *in vivo* using a Balb/c mouse xenograft model of invasive B16-F10 melanoma. The results are shown in Figure 8. Complex **10** was administered intraperitoneally to the mice twice on two consecutive days (each time 7.5 mg/kg body weight on days 1, 2, 7, and 8). This induced a considerable reduction in tumor volumes to 18-48% of the initial size after twelve days while the volumes of untreated B16-F10 tumors increased by 1.6- to 1.9-fold. The weight of the mice remained nearly the same as at the beginning of the experiment. Thus, it can be concluded from this preliminary study that complex **10** exhibits a significant *in vivo* antitumor activity against this type of highly metastatic melanoma while being tolerated very well by the mice.

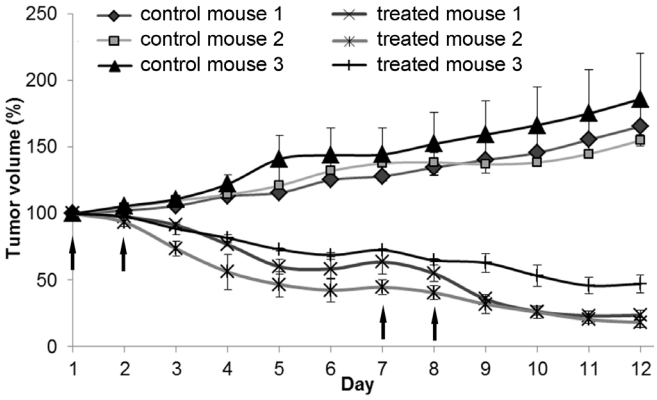

Figure 8. Antitumoral activity of complex **10** in mouse xenografts of the highly metastatic B16-F10 melanoma cell line. Shown are the relative tumor responses following a repeated application of DMSO (control) or complex **10** on two concecutive days (i.p. injections of 7.5 mg/kg body weight on days 1, 2, 7, and 8: black arrows). Data are means ± SD of the tumors implanted in both flanks of each mouse.

Conclusions

The ferrocenyl substituted NHC gold(I) complexes **7a**, **7b**, **8**, and **10** showed activity against various tumor cell entities with IC_{50} values in the lower micromolar or even submicromolar range. In xenografted mice complex **10** led to significant reductions of the tumor volumes while being tolerated well by the animals. The cytotoxicity of the complexes is correlated with their cellular uptake, which is dependent on their lipophilicity. The mechanism of action of complexes **8** and **10** was studied in detail. They induced a distinct reorganization of the F-actin cytoskeleton in human vascular endothelial and melanoma cells, which was associated with an accumulation of the cells in the G1 phase of the cell cycle leading to a significant antimigratory effect. Moreover, complexes **8** and **10** are potent inhibitors of the redox enzyme TrxR with complex **8** being about 2.5 times more effective than complex **10**. This is in line with findings by Rubbiani *et al.* for similar gold(I) NHC complexes and is most likely due to the lower stability of complex **8** leading to a higher reactivity toward nucleophiles present in the active site of the TrxR enzyme.[23,38] Our results indicate that not only the inhibition of TrxR but also the presence of the ROS regulating/producing ferrocene moieties in complexes **8** and **10** are responsible for the observed increase in the cellular ROS levels. The accumulation of ROS in the investigated melanoma cells was also associated with a decrease in the mitochondrial membrane potential. Such antimitochondrial effects are typical of agents that alter the intracellular redox homeostasis.[45–48] The complexes **8** and **10** also showed distinct antivascular effects, such as an inhibition of the formation of vessel-like structures by HUVEC *in vitro*, and a disruption of the vasculature in the CAM of fertilized chicken eggs. This pleiotropic spectrum of anticancer effects *in vitro* and *in vivo* makes these new heteronuclear NHC complexes promising drug candidates. We will now study their effects on cancer-relevant signal transduction pathways by proteomic techniques known to be applicable to gold complexes such as ELISA microarray analyses[58,59] or two-dimensional difference gel electrophoresis.[60]

Experimental Section

General: Melting points are uncorrected; IR spectra were recorded on an FT-IR spectrophotometer with ATR sampling unit; NMR spectra were run on 300 and 500 MHz spectrometers; chemical shifts are given in ppm (δ) downfield from tetramethylsilane as internal standard for ^{1}H and ^{13}C; mass spectra: direct inlet, EI, 70 eV; HRMS: UPLC/Orbitrap MS system in ESI mode; microanalyses: Vario EL III elemental analyser. All tested compounds are > 98% pure by elemental analysis and HPLC. For *in vitro* tests stock solutions of the complexes in DMF, stable for months, were prepared.

Chemistry. 1-Methyl-5-ferrocenyl-4-phenylimidazole (4a): Ferrocenyl carboxaldehyde (90 mg, 0.42 mmol) was dissolved in ethanol (15 mL), treated with 33% $MeNH_2$/EtOH (260 µL, 2.10 mmol) and acetic acid (150 µL, 2.63 mmol), and heated for 2 h under reflux. TosMIC reagent **3** (120 mg, 0.44 mmol) and K_2CO_3 (500 mg, 3.62 mmol) were added and the reaction mixture was stirred for 6 h under reflux. The volatiles were evaporated and the residue was suspended in ethyl acetate, washed with water, dried over Na_2SO_4, filtered, and the filtrate was concentrated in vacuum. The residue was purified by column chromatography (silica gel 60). Yield: 75 mg (0.32 mmol, 76%); orange-brown solid; R_f=0.44 (ethyl acetate); ^{1}H NMR (300 MHz, $CDCl_3$) δ=3.93 (s, 3H), 4.0–4.1 (m, 5H), 4.2–4.3 (m, 4H), 7.2–7.4 (m, 3H), 7.4–7.5 ppm (m, 3H); ^{13}C NMR (75.5 MHz, $CDCl_3$) δ=32.8, 68.1, 68.7, 69.0, 75.3, 126.6, 127.8, 128.7, 130.6, 135.6, 137.8, 140.2 ppm; ν_{max}/cm^{-1}: 3086, 2923, 1603, 1511, 1442, 1415, 1392, 1374, 1322, 1285, 1254, 1204, 1156, 1103, 1088, 1070, 1031, 998, 955, 915, 889, 867, 834, 824, 811, 774, 752, 719, 697, 663; MS (70eV): *m/z* (%) 342 (100) [M$^+$], 277 (25), 234 (26), 220 (75), 165 (42).

1-Ethyl-5-ferrocenyl-4-phenylimidazole (4b): Ferrocenyl carboxaldehyde (90 mg, 0.42 mmol) was dissolved in ethanol (15 mL), treated with 2M $EtNH_2$/THF (1.05 mL, 2.10 mmol) and acetic acid (150 µL, 2.63 mmol), and heated for 2 h under reflux. Compound **3** (120 mg, 0.44 mmol) and K_2CO_3 (500 mg, 3.62 mmol) were added and the reaction mixture was heated for 6 h under reflux. The solvent was evaporated and the residue was suspended in ethyl acetate, washed with water, dried over Na_2SO_4, filtered, and the filtrate was concentrated in vacuum. The residue was purified by column chromatography (silica gel 60). Yield: 100 mg (0.28 mmol, 67%); orange-brown solid; R_f=0.77 (ethyl acetate/methanol 9:1); ^{1}H NMR (300 MHz, $CDCl_3$) δ=1.51 (t, J = 7.3 Hz, 3H), 3.9–4.0 (m, 5H), 4.2–4.3 (m, 4H), 4.43 (q, J = 7.3 Hz, 2H), 7.1–7.3 (m, 3H), 7.4–7.5 (m, 2H), 7.57 (s, 1H); ^{13}C NMR (75.5 MHz, $CDCl_3$) δ=16.9, 39.8, 68.1, 68.9, 69.0, 75.3, 124.2, 126.5, 127.7, 128.7, 130.7, 135.6, 136.1, 140.0; ν_{max}/cm^{-1}: 3089, 2974, 2933, 1602, 1506, 1442, 1411, 1378, 1347, 1250, 1199, 1105, 1070, 1029, 1000, 948, 912, 875, 819, 771, 721, 697, 662; MS (70 eV): *m/z* (%) 356 (100) [M$^+$], 291 (15), 248 (88), 219 (25), 165 (27), 89 (21).

1,3-Dimethyl-5-ferrocenyl-4-phenylimidazolium iodide (5a): Compound **4a** (70 mg, 0.20 mmol) was dissolved in acetonitrile (25 mL) and iodomethane (3 mL) was added. The reaction mixture was stirred at 85 °C for 24 h. The solvent was evaporated and the residue was dried in vacuum. Yield: 97 mg (0.20 mmol, 100%); yellow gum; ^{1}H NMR (300 MHz, $CDCl_3$) δ=3.6–4.3 (m, 15H), 7.2–7.5 (m, 5H), 9.84 (s, 1H); ^{13}C NMR (75.5 MHz, $CDCl_3$) δ=34.7, 35.8, 68.3, 68.7, 69.4, 125.5, 128.7, 128.9, 130.4, 136.9; ν_{max}/cm^{-1}: 3460, 3146, 3020, 1621, 1573, 1489, 1440, 1409, 1343, 1202, 1105, 1086, 1058, 1004, 918, 893, 817, 763, 725, 703; MS (70 eV): *m/z* (%) 357 (92) [M$^+$], 342 (100), 277 (34), 234 (49), 142 (52), 121 (14).

1,3-Diethyl-5-ferrocenyl-4-phenylimidazolium iodide (5b): Compound **4b** (100 mg, 0.28 mmol) was dissolved in acetonitrile (25 mL) and iodoethane (1.5 mL) was added. The reaction mixture was stirred at 85 °C for 24 h. The solvent was evaporated and the residue was dried in vacuum. Yield: 130 mg (0.25 mmol, 89%); yellow gum; ^{1}H NMR (300 MHz, $CDCl_3$) δ=1.31 (t, J = 7.2 Hz, 3H), 1.63 (t, J = 7.2 Hz, 3H), 3.7–3.8 (m, 5H), 4.0–4.1 (m, 4H), 4.1–4.2 (m, 2H), 4.56 (q, J = 7.2 Hz, 2H), 7.2–7.5 (m, 5H), 10.01 (s, 1H); ^{13}C NMR (75.5 MHz, $CDCl_3$) δ=15.3, 15.9, 42.9, 43.1, 68.5, 59.2, 69.3, 69.5, 124.3, 125.5, 128.8, 129.0, 129.8, 129.9, 130.2, 130.3, 130.4, 130.7, 134.9, 138.0; ν_{max}/cm^{-1}: 3050, 2979, 1936, 1617, 1561, 1444, 1410, 1386, 1342, 1220, 1182, 1105, 1090, 1074, 1024, 1002, 918, 883, 819, 757, 724, 701, 639; MS (70 eV): *m/z* (%) 356 (100), 291 (10), 248 (15).

Iodido-(1,3-dimethyl-4-ferrocenyl-5-phenylimidazol-2-ylidene)-silver(I) (6a): A mixture of imidazolium salt **5a** (95 mg, 0.20 mmol), CH_2Cl_2 (15 mL), and silver(I) oxide (46 mg, 0.20 mmol) was stirred at room temperature in the dark for 1 d. The suspension was filtered over Celite and the filtrate was concentrated in vacuum. The residue was dissolved in CH_2Cl_2 and the product precipitated with *n*-hexane. Yield: 72 mg (0.12 mmol, 61%); brown gum; ^{1}H NMR (300 MHz, $CDCl_3$) δ=3.55 (s, 6H), 3.9–4.3 (m, 9H), 7.2–7.5 (m, 5H); ^{13}C NMR (75.5 MHz, $CDCl_3$) δ=37.4, 38.2, 68.2, 68.8, 69.3, 72.9, 128.7, 128.9, 129.5, 130.3, 130.8, 131.3, 179.8; ν_{max}/cm^{-1}: 3085, 2947, 1622, 1595, 1574, 1503, 1445, 1377, 1254, 1222, 1105, 1077, 1060, 1034, 1015, 911, 896, 820, 764, 723, 700; MS (70 eV): *m/z* (%) 342 (45), 234 (38), 186 (99), 121 (91), 57 (38).

Iodido-(1,3-diethyl-4-ferrocenyl-5-phenylimidazol-2-ylidene)silver(I) (6b): Analogously to **6a**, compound **6b** (90 mg, 0.15 mmol, 60%) was obtained from **5b** (130 mg, 0.25 mmol), CH_2Cl_2 (15 mL), and silver(I) oxide (65 mg, 0.28 mmol) as a brown gum; ^{1}H NMR (300 MHz, $CDCl_3$) δ=1.13 (t, J = 7.2 Hz, 3H), 1.47 (t, J = 7.2 Hz, 3H), 3.8–3.9 (m, 7H), 3.9–4.0 (m, 2H), 4.1–4.2 (m, 2H), 4.48 (q, J = 7.2 Hz, 2H), 7.2–7.3 (m, 3H), 7.4–7.5 (m, 2H); ^{13}C NMR (75.5 MHz, $CDCl_3$) δ=17.2, 18.1, 44.5, 44.7, 68.2, 68.7, 69.1, 72.8, 127.7, 128.3, 128.6, 128.8, 129.5, 130.2, 131.5, 133.8, 177.8; ν_{max}/cm^{-1}: 3084, 2970, 2928, 2865, 1499, 1459, 1443, 1398, 1375, 1343, 1306, 1254, 1212, 1105, 1094, 1072, 1049, 1026, 1001, 965, 919, 883, 821, 799, 757, 728, 701; MS (70 eV): *m/z* (%) 620 (1) [M$^+$], 618 (1) [M$^+$], 528 (2), 526 (2), 383 (71), 356 (68), 275 (100), 247 (59), 219 (16), 186 (20), 165 (18).

Chlorido-(1,3-dimethyl-4-ferrocenyl-5-phenylimidazol-2-ylidene)gold(I) (7a): Complex **6a** (70 mg, 0.12 mmol) was dissolved in CH_2Cl_2 (15 mL) and treated with chloro(dimethylsulfide)gold(I) (49 mg, 0.16 mmol). The reaction mixture was stirred at room temperature for 18 h. The suspension was filtered, the filtrate was concentrated in vacuum and the residue recrystallised from CH_2Cl_2/*n*-hexane. Yield: 60 mg (0.10 mmol, 86%); amber solid of m.p. 120 °C; ^{1}H NMR (500 MHz, CD_2Cl_2) δ=3.59 (s, 3H), 4.05 (s, 5H), 4.10 (m, 2H), 4.16 (s, 3H), 4.25 (m, 2H), 7.28 (m, 2H), 7.51 (m, 3H); ^{13}C NMR (125 MHz, CD_2Cl_2) δ=38.1, 68.9, 69.5, 69.9, 129,4, 129.6, 130.2, 131.6, 170.7; ν_{max}/cm^{-1}: 3087, 2948, 1621, 1595, 1575, 1445, 1382, 1266, 1218, 1121, 1106, 1081, 1058, 1004, 927, 898, 821, 767, 701, 671; MS (70 eV): *m/z* (%) 588 (65) [M$^+$], 480 (54), 455 (100), 342 (79), 186 (100), 121 (40), 66 (57), 57 (36); elemental analysis calcd (%) for $C_{21}H_{20}AuClFeN_2$ (588.66): C 43.85, H 3.42, N 4.76; found: C 43.89, H 4.01, N 5.20.

Chlorido-(1,3-diethyl-4-ferrocenyl-5-phenylimidazol-2-ylidene)gold(I) (7b): Analogously to **7a** complex **7b** (60 mg, 0.097 mmol, 81%) was obtained from **6b** (75 mg, 0.12 mmol), CH_2Cl_2 (15 mL), and chloro(dimethylsulfide)gold(I) (36 mg, 0.12 mmol) as an amber solid of m.p. 85–87 °C; ^{1}H NMR (500 MHz, $CDCl_3$) δ=1.22 (t, J = 7.2 Hz, 3H), 1.58 (t, J = 7.2 Hz, 3H), 3.99 (s, 5H), 4.08 (m, 4H), 4.22 (m, 2H), 4.67 (m, 2H), 7.33 (m, 2H), 7.49 (m, 3H); ^{13}C NMR (75.5 MHz, $CDCl_3$) δ=16.8, 17.6, 44.1, 44.2, 68.4, 69.0, 69.5, 69.7, 72.7, 127.9, 128.5, 128.8, 129.1, 129.4, 129.8, 129.9, 130.4, 131.1, 133.8, 169.2; ν_{max}/cm^{-1}: 2964, 2932, 1623, 1593, 1504, 1461, 1444, 1409, 1377, 1345, 1308, 1262, 1214, 1106, 1094, 1026, 1000, 967, 919, 885, 822, 758, 727, 702; MS (70 eV): *m/z* (%) 618 (18) [M$^+$], 616 (47) [M$^+$], 508 (52), 471 (45), 275 (51), 66 (100); elemental analysis calcd (%) for $C_{23}H_{24}AuClFeN_2$ (616.71): C 44.79, H 3.92, N 4.54; found: C 45.09, H 3.93, N 4.79.

Triphenylphosphino-(1,3-diethyl-4-ferrocenyl-5-phenylimidazol-2-ylidene)gold(I) tetrafluoroborate (8): Complex **7b** (45 mg, 0.073 mmol) was dissolved in acetone (10 mL) and treated with $NaBF_4$ (15 mg, 0.136 mmol) and PPh_3 (25 mg, 0.095 mmol). The reaction mixture was stirred at room temperature for 1 h. The suspension was filtered, the filtrate was concentrated in vacuum and the residue recrystallised from CH_2Cl_2/*n*-hexane. Yield: 50 mg (0.054 mmol, 74%); amber solid of m.p. 183 °C (dec.); ^{1}H NMR (500 MHz, $CDCl_3$) δ=1.33 (dt, J = 14.6, 7.2 Hz, 3H), 1.70 (dt, J = 14.6, 7.2 Hz, 3H), 4.04 (s, 5H), 4.13 (m, 4H), 4.28 (m, 2H), 4.73 (m, 2H), 7.37 (m, 3H), 7.58 (m, 17H); ^{13}C NMR (125 MHz, $CDCl_3$) δ=17.4, 18.3, 18.4, 44.2, 44.5, 68.5, 68.6 69.1, 69.5, 72.0, 72.5, 128.2, 128.6, 129.2, 129.3, 129.5, 129.8, 129.9, 130.0, 130.1, 130.6, 131.2, 132.4, 133.8, 134.1, 134.2, 182.8; ^{31}P NMR (202 MHz, $CDCl_3$) δ 41.0; ^{11}B NMR (96.3 MHz, $CDCl_3$) δ= –1.18; ν_{max}/cm^{-1}: 3059, 2963, 1480, 1464, 1436, 1413, 1379, 1344, 1306, 1183, 1159, 1098, 1049, 997, 925, 884, 823, 748, 693; MS (70 eV): *m/z* (%) 843.3 (100) [M$^+$ -BF_4], 735.4 (15), 721.3 (49), 385.3 (24), 338 (16), 279 (13); elemental analysis calcd (%) for $C_{41}H_{39}AuBF_4FeN_2P$ (930.35): C 52.93, H 4.23, N 3.01; found: C 53.10, H 4.50, N 3.36.

1,3-Diethyl-4-ferrocenyl-5-phenylimidazolium tetrafluoroborate (9): A mixture of **5b** (67 mg, 0.13 mmol), acetone (30 mL), and $NaBF_4$ (22 mg, 0.20 mmol) was stirred at room temperature for 24 h. The mixture was filtered over $MgSO_4$, the filtrate was concentrated in vacuum and the residue was dried. Yield: 60 mg (0.13 mmol, 100%); yellow gum; ^{1}H NMR (300 MHz, $CDCl_3$) δ=1.40 (t, J = 7.3 Hz, 3H), 1.72 (t, J = 7.3 Hz, 3H), 3.9–4.0 (m, 5H,), 4.0–4.1 (m, 4H), 4.3–4.4 (m, 2H), 4.66 (q, J = 7.3 Hz, 2H), 7.3–7.4 (m, 2H), 7.5–7.7 (m, 3H), 10.18 (s, 1H); ^{13}C NMR (75.5 MHz, $CDCl_3$) δ=15.6, 16.3, 44.3, 44.4, 68.8, 69.2, 69.6, 69.9, 70.2, 126.0, 129.2, 129.4, 129.7, 130.1, 130.2, 130.5, 130.6, 130.8, 131.0, 135.5, 148.5; ν_{max}/cm^{-1}: 3055, 2978, 2936, 1615, 1561, 1444, 1410, 1386, 1342, 1220, 1181, 1105, 1024, 1002, 918, 883, 819, 794, 757, 725, 702; MS(70 eV): *m/z* (%) 356 (100), 291 (15), 248 (22).

Bis-[1,3-diethyl-4-ferrocenyl-5-phenylimidazol-2-ylidene]gold(I) tetrafluoroborate (10): Imidazolium salt **9** (60 mg, 0.13 mmol) was dissolved in CH_2Cl_2/methanol (1:1, 30 mL) and treated with Ag_2O (34 mg, 0.14 mmol). The resulting mixture was stirred in the dark at room temperature for 5 h. Chloro(dimethylsulfide)gold(I) (23 mg, 0.075 mmol) was added and stirring was continued for a further 20 h. The suspension was filtered, the filtrate was concentrated in vacuum, and the residue was redissolved in CH_2Cl_2, and filtered over $MgSO_4$/celite. The filtrate was concentrated and the remainder was dried in vacuum. Yield: 50 mg (0.05 mmol, 64%); amber solid of m.p. 183 °C (dec.); ^{1}H NMR (300 MHz, $CDCl_3$) δ=1.1–1.3 (m, 6H), 1.6–1.8 (m, 6H), 3.8–4.3 (m, 22H), 4.6–4.8 (m, 4H), 7.1–7.6 (m, 10H); ^{13}C NMR (75.5 MHz, $CDCl_3$) δ=16.8, 17.3, 17.6, 18.2, 44.1, 44.2, 68.5, 69.0, 69.1, 69.3, 69.4, 72.4, 72.8, 128.0, 128.5, 128.9, 129.1, 129.4, 129.8, 130.5, 130.8, 131.2, 131.8, 135.0, 161.2, 182.7; ^{11}B NMR (96.3 MHz, $CDCl_3$) δ= –1.29; ν_{max}/cm^{-1}: 2972, 2924, 1462, 1446, 1411, 1378, 1345, 1306, 1262, 1216, 1195, 1107, 1050, 1002, 969, 885, 834, 818, 757, 703; MS (70 eV): *m/z* (%) 965.2 (100) [M$^+$ –BF_4], 857.4 (6), 506.8 (7), 338.5 (23), 282.4 (7); elemental analysis calcd (%) for $C_{46}H_{48}AuBF_4Fe_2N_4$ (1052.36): C 52.50, H 4.60, N 5.32; found: C 52.48, H 4.55, N 5.02.

Crystal data: $C_{46}H_{48}AuBF_4Fe_2N_4$, M=1052.36, monoclinic, space group C2/c, a=19.657(4), b=10.889(2), c=21.868(4) Å, α=γ=90°, β=114.33(3)°, V=4264.8(15) Å^3, Z=4, λ=0.71073 Å, μ=4.158 mm^{-1}, T=293(2) K; 15540 reflections measured, 4121 unique; final refinement to convergence on F^2 gave R=0.0539 and Rw=0.1161, GOF=0.703. CCDC 1500972.

Biological Studies. **Enzyme**: PARP-1 activity was determined using Trevigen's HT universal colorimetric PARP assay according to the

manufacturer's instructions. It measures the incorporation of biotinylated poly(ADP-ribose) in histone proteins in a 96-microtiter strip well format. Recombinant human PARP-1 (high specific activity, purified from *E. coli* containing recombinant plasmid harboring the human PARP gene) was used as the enzyme source and incubated with different concentrations of complexes **8** and **10** for 1 h at room temperature prior to its addition to the histone proteins in the 96-well plates. The final reaction mixture (50 µL) was treated with TACS-Sapphire, a horseradish peroxidase colorimetric substrate, and incubated in the dark for 30 min. The absorbance was measured at 630 nm. The experiment was performed twice in duplicate and EC_{50} values are presented as means ± S.D..

The inhibition of thioredoxin reductase (TrxR) by **8** and **10** was assessed using a microplate reader based assay with minor modifications.[4,38,61] Rat liver TrxR (Sigma-Aldrich) was diluted with water to a concentration of 2.0 U/mL. To 25 µL aliquots of the enzyme solution 25 µL of potassium phosphate buffer pH 7.0 containing the complexes **8** and **10** in graded concentrations or vehicle (DMF) were added. The resulting solutions (final concentration of DMF: 0.5% v/v) were incubated for 75 min at 37 °C in a 96-well plate. To each well, 225 µL of the reaction mixture (1000 µL reaction mixture: 500 µL potassium phosphate buffer pH 7.0, 80 µL 100 mM EDTA solution pH 7.5, 20 µL BSA solution 0.05%, 100 µL of 20mM NADPH solution, and 300 µL of distilled water) were added and the reaction was started by adding 25 µL of a 20 mM DTNB solution. The formation of 5-TNB was monitored with a Perkin-Elmer Victor X4 microplate reader at 405 nm in 10 s intervals for 6 min. The increase in 5-TNB concentrations over time followed a linear trend ($r^2 \geq 0.99$), and the enzymatic activities were calculated as the slopes (increase in absorbance per second) thereof. The noninterference of the test compounds with the assay components was confirmed by negative control experiments with enzyme-free solution. The EC_{50} values are the complex concentrations decreasing the enzymatic activity to 50%, given as means ± S.D. of two or three experiments in duplicate.

Tube Formation Assay: The interference of **8** and **10** with the formation of vascular-like tubular networks by HUVEC was investigated *in vitro*. HUVEC (25 µL of 8×10^5 cells/mL) were seeded on matrigel (BD Biosciences) in black 96-well plates and treated with **8** or **10** (dilution of 10 mM stock solutions in DMF ranging from 50 nM to 10 µM in H_2O) to identify antiangiogenic activity. Solvent controls (DMF) were treated identically. Effects were documented by light microscopy after 24 h of incubation (Axiovert 35, 5× objective lens, AxioCam color, Zeiss).[9,53,62]

Chorioallantoic Membrane (CAM) Assay: Fertilized, specific pathogen-free (SPF) chicken eggs (VALO BioMedia) were bred in an incubator at 37 °C and 60% relative humidity. On day 6 windows (Ø 1.5–2 cm) were cut into the shell at the more rounded pole of the egg. The holes were sealed with tape, and incubation was continued overnight. Rings of silicon foil (Ø 5 mm) were placed on the CAM with its developing blood vessels, and complexes **8** or **10** (2.5 nmol), or DMF as control (all in a volume of 10 µL H_2O) were topically applied within the rings. The effects on the developing vasculature were documented after incubation for 6 h and 24 h using a light microscope (60× magnification, Traveler). The fractal analyses to quantify a decrease in areas covered by blood vessels after 6 h of incubation with the test compounds was carried out as described before using ImageJ 1.48f (FracLac_2015Jul plugin) and the Fractal Analysis System 3.4.7 software.[9]

Mouse Xenograft Model: The animal studies had been approved by the committee on animal care (Government of Rhineland–Palatinate). The mice (Balb/c) were kept under a 12 h light–dark cycle in a controlled conventional colony room. They had free access to sterilized water and standard rodent diet ad libitum. They were sacrificed by cervical dislocation corresponding to the guidelines of the committee on animal care. To analyze the *in vivo* antitumor activity and tolerance of gold complex **10**, a Balb/c mouse xenograft model of highly metastatic B16-F10 mouse melanoma cells was used. A suspension of 2×10^5 cells in 200 mL PBS was administered to the flanks of each mouse to generate subcutaneous xenograft tumors. Freshly prepared 9 mM stock solutions of complex **10** in DMSO were diluted 1:9 with PBS and injected i.p. twice on two consecutive days (days 1, 2, and 7, 8) in the mice (n=3) at 7.5 mg × (kg body weight)$^{-1}$. Control mice (n=3) were treated with respective amounts of DMSO (in PBS). The size of the tumors was recorded daily, beginning on the day of the first injection. Tumor volumes were calculated by the formula $a^2 \times b \times 0.5$, with *a* being the short and *b* the long dimension. The weight of the mice was measured at the beginning (day 1) and at the end of the experiment (day 12) and was used as an indication of drug tolerance.

Further tests: For details on the studies of growth inhibition, cellular accumulation, partition coefficients, interference with F-actin and mitochondrial membrane potential, cell cycle, wound healing, and ROS generation refer to the Supporting information.

Acknowledgements

We thank the COST Action CM1105 'Functional metal complexes that bind to biomolecules' for support and an STSM appropriation (JKM), RS thanks the Deutsche Forschungs-gemeinschaft for a grant (Scho 402/12), VB and OS thank the Czech Science Foundation for a grant (14-21053S), and JKM thanks the Elite Study Program 'Macromolecular Science', Elite Network of Bavaria. We are indebted to Friedrich Foerster (Institute of Translational Immunology, University Medical Center of the Johannes Gutenberg-University Mainz, Germany) for kindly providing B16-F10 melanoma cells and to Katja Dankhoff (University Bayreuth) for assistance with the cyclic voltammetry.

Keywords: antitumor agents • carbenes • metal-based drugs • gold • antivascular activity

[1] K. D. Mjos, C. Orvig, *Chem. Rev.* **2014**, *114* (8), 4540–4563.
[2] I. Ott, Biodistribution of metals and metallodrugs. In *Comprehensive Inorganic Chemistry II*, Elsevier, **2013**; pp 933–949.
[3] W. Liu, R. Gust, *Chem. Soc. Rev.* **2013**, *42* (2), 755–773.
[4] I. Ott, X. Qian, Y. Xu, D. H. W. Vlecken, I. J. Marques, D. Kubutat, J. Will, W. S. Sheldrick, P. Jesse, A. Prokop, C. P. Bagowski, *J. Med. Chem*. **2009**, *52* (3), 763–770.
[5] A. Meyer, L. Oehninger, Y. Geldmacher, H. Alborzinia, S. Wölfl, W. S. Sheldrick, I. Ott, *ChemMedChem* **2014**, 1794–1800.
[6] L. Oehninger, R. Rubbiani, I. Ott, *Dalton Trans.* **2013**, *42* (10), 3269–3284.
[7] L. Kaps, B. Biersack, H. Müller-Bunz, K. Mahal, J. Muenzner, M. Tacke, T. Mueller, R. Schobert, *J. Inorg. Biochem.* **2012**, *106* (1), 52–58.
[8] J. K. Muenzner, B. Biersack, L. Kaps, K. Mahal, R. Schobert, F. Sasse, *Int. J. Clin. Pharmacol. Ther.* **2013**, *51* (1), 44–46.
[9] J. K. Muenzner, B. Biersack, H. Kalie, I. C. Andronache, L. Kaps, D. Schuppan, F. Sasse, R. Schobert, *ChemMedChem* **2014**, *9* (6), 1195–1204.
[10] N. P. Farrell, S. G. D. Almeida, K. A. Skov, *J. Am. Chem. Soc.* **1988**, *110* (15), 5018–5019.
[11] N. Lease, V. Vasilevski, M. Carreira, A. de Almeida, M. Sanaú, P. Hirva, A. Casini, M. Contel, *J. Med. Chem.* **2013**, *56* (14), 5806–5818.
[12] K. Wang, E. Gao, *Anticancer Agents Med. Chem.* **2014**, *14* (1), 147–169.
[13] B. Bertrand, A. Citta, I. L. Franken, M. Picquet, A. Folda, V. Scalcon, M. P. Rigobello, P. Le Gendre, A. Casini, E. Bodio, *J. Biol. Inorg. Chem.* **2015**, *20* (6), 1005–1020.

[14] R. Kovjazin, T. Eldar, M. Patya, A. Vanichkin, H. M. Lander, A. Novogrodsky, *FASEB J.* **2003**, *17* (3), 467–469.

[15] S. Top, A. Vessieres, G. Leclercq, J. Quivy, J. Tang, J. Vaissermann, M. Huche, G. Jaouen, *Chem. Weinh. Bergstr. Ger.* **2003**, *9* (21), 5223–5236.

[16] L. V. Snegur, Y. S. Nekrasov, N. S. Sergeeva, Z. V. Zhilina, V. V. Gumenyuk, Z. A. Starikova, A. A. Simenel, N. B. Morozova, I. K. Sviridova, V. N. Babin, *Appl. Organomet. Chem.* **2008**, *22* (2), 139–147.

[17] A. A. Simenel, E. A. Morozova, L. V. Snegur, S. I. Zykova, V. V. Kachala, L. A. Ostrovskaya, N. V. Bluchterova, M. M. Fomina, *Appl. Organomet. Chem.* **2009**, *23* (6), 219–224.

[18] S. Knauer, B. Biersack, M. Zoldakova, K. Effenberger, W. Milius, R. Schobert, *Anticancer Drugs* **2009**, *20* (8), 676–681.

[19] C. Ornelas, *New J. Chem.* **2011**, *35* (10), 1973.

[20] M. C. Gimeno, H. Goitia, A. Laguna, M. E. Luque, M. D. Villacampa, C. Sepúlveda, M. Meireles, *J. Inorg. Biochem.* **2011**, *105* (11), 1373–1382.

[21] W. Liu, K. Bensdorf, M. Proetto, A. Hagenbach, U. Abram, R. Gust, *J. Med. Chem.* **2012**, *55* (8), 3713–3724.

[22] T. Mosmann, *J. Immunol. Methods* **1983**, *65*, 55–63.

[23] R. Rubbiani, S. Can, I. Kitanovic, H. Alborzinia, M. Stefanopoulou, M. Kokoschka, S. Mönchgesang, W. S. Sheldrick, S. Wölfl, I. Ott, *J. Med. Chem.* **2011**, *54* (24), 8646–8657.

[24] M. Alvarez, R. Robey, V. Sandor, K. Nishiyama, Y. Matsumoto, K. Paull, S. Bates, T. Fojo, *Mol. Pharmacol.* **1998**, *54* (5), 802–814.

[25] J. Cummings, N. Zelcer, J. D. Allen, D. Yao, G. Boyd, M. Maliepaard, T. H. Friedberg, J. F. Smyth, D. I. Jodrell, *Biochem. Pharmacol.* **2004**, *67* (1), 31–39.

[26] L. A. Doyle, W. Yang, L. V. Abruzzo, T. Krogmann, Y. Gao, A. K. Rishi, D. D. Ross, *Proc. Natl. Acad. Sci.* **1998**, *95* (26), 15665–15670.

[27] M. Kühnle, M. Egger, C. Müller, A. Mahringer, G. Bernhardt, G. Fricker, B. König, A. Buschauer, *J. Med. Chem.* **2009**, *52* (4), 1190–1197.

[28] A. Fojo, S. Akiyama, M. M. Gottesman, I. Pastan, *Cancer Res.* **1985**, *45* (7), 3002–3007.

[29] D.-W. Shen, C. Cardarelli, J. Hwang, M. Cornwell, N. Richert, S. Ishii, I. Pastan, M. M. Gottesman, *J. Biol. Chem.* **1986**, *261* (17), 7762–7770.

[30] M. C. Willingham, M. M. Cornwell, C. O. Cardarelli, M. M. Gottesman, I. Pastan, *Cancer Res.* **1986**, *46* (11), 5941–5946.

[31] S. P. Oldfield, M. D. Hall, J. A. Platts, *J. Med. Chem.* **2007**, *50* (21), 5227–5237.

[32] Z. Liu, L. Salassa, A. Habtemariam, A. M. Pizarro, G. J. Clarkson, P. Sadler, *Inorg. Chem.* **2011**, *50* (12), 5777–5783.

[33] E. A. Papakonstanti, C. Stournaras, *FEBS Lett.* **2008**, *582* (14), 2120–2127.

[34] L. L. Lohmer, L. C. Kelley, E. J. Hagedorn, D. R. Sherwood, *Cell Adhes. Migr.* **2014**, *8* (3), 246–255.

[35] T. Bonello, J. Coombes, G. Schevzov, P. Gunning, J. Stehn, M. Kavallaris, Therapeutic targeting of the actin cytoskeleton in cancer. In *Cytoskeleton and Human Disease*; Kavallaris, M., Ed.; Humana Press, **2012**, pp 181–200.

[36] J. Nordberg, E. S. Arner, *Free Radic. Biol. Med.* **2001**, *31* (11), 1287–1312.

[37] J. E. Biaglow, R. A. Miller, *Cancer Biol. Ther.* **2005**, *4* (1), 13–20.

[38] R. Rubbiani, I. Kitanovic, H. Alborzinia, S. Can, A. Kitanovic, L. A. Onambele, M. Stefanopoulou, Y. Geldmacher, W. S. Sheldrick, G. Wolber, A. Prokop, S. Wölfl, I. Ott, *J. Med. Chem.* **2010**, *53* (24), 8608–8618.

[39] R. Rubbiani, E. Schuh, A. Meyer, J. Lemke, J. Wimberg, N. Metzler-Nolte, F. Meyer, F. Mohr, I. Ott, *Med. Chem. Commun.* **2013**, *4* (6), 942–948.

[40] S. M. Meier, C. Gerner, B. K. Keppler, M.A. Cinellu, A. Casini, *Inorg. Chem*. **2016**, *55*, 4248−4259.

[41] A. Pratesi, C. Gabbiani, M. G., L. Messori, *Chem. Commun*., **2010**, *46*, 7001–7003.

[42] F. Mendes, M. Groessl, A. A. Nazarov, Y. O. Tsybin, G. Sava, I. Santos, P. J. Dyson, A. Casini, *J. Med. Chem.* **2011**, *54* (7), 2196–2206.

[43] M. Serratrice, F. Edafe, F. Mendes, R. Scopelliti, S. M. Zakeeruddin, M. Grätzel, I. Santos, M. A. Cinellu, A. Casini, *Dalton Trans.* **2012**, *41* (11), 3287.

[44] W. I. Pérez, Y. Soto, C. Ortíz, J. Matta, E. Meléndez, *Bioorg. Med. Chem.* **2015**, *23* (3), 471–479.

[45] M. P. Rigobello, L. Messori, G. Marcon, M. Agostina Cinellu, M. Bragadin, A. Folda, G. Scutari, A. Bindoli, *J. Inorg. Biochem.* **2004**, *98* (10), 1634–1641.

[46] M. P. Rigobello, G. Scutari, A. Folda, A. Bindoli, *Biochem. Pharmacol.* **2004**, *67* (4), 689–696.

[47] M. Bragadin, G. Scutari, A. Folda, A. Bindoli, M. P. Rigobello, *Ann. N. Y. Acad. Sci.* **2004**, *1030* (1), 348–354.

[48] P. J. Barnard, S. J. Berners-Price, *37th Int. Conf. Coord. Chem. Cape Town South Afr.* **2007**, *251* (13–14), 1889–1902.

[49] S. Elmore, *Toxicol. Pathol.* **2007**, *35* (4), 495–516.

[50] I. Ott, *Coord. Chem. Rev.* **2009**, *253*, 1670–1681.

[51] J. S. Modica-Napolitano, J. R. Aprille, *Adv. Drug Deliv. Rev.* **2001**, *49*, 63–70.

[52] S. Spreckelmeyer, C. Orvig, A. Casini, *Molecules* **2014**, *19* (10), 15584–15610.

[53] M. Ponce, Tube formation: an in vitro matrigel angiogenesis assay. In *Angiogenesis Protocols*; Murray, C., Martin, S., Eds.; Methods in Molecular Biology; Humana Press, **2009**, Vol. 467, pp 183–188.

[54] D. Ribatti, B. Nico, A. Vacca, L. Roncali, P. H. Burri, V. Djonov, *Anat. Rec.* **2001**, *264* (4), 317–324.

[55] K. Norrby, *Cell. Mol. Med.* **2006**, *10* (3), 588–612.

[56] P. Nowak-Sliwinska, T. Segura, M. L. Iruela-Arispe, *Angiogenesis* **2014**, *17* (4), 779–804.

[57] L. M. Kirchner, S. P. Schmidt, B. S. Gruber, *Microvasc. Res.* **1996**, *51* (1), 2–14.

[58] X. Cheng, P. Holenya, S. Can, H. Alborzinia, R. Rubbiani, I. Ott., S. Wölfl, *Molecular Cancer* **2014**, *13*:221.

[59] P. Holenya, S. Can, R. Rubbiani, H. Alborzinia, A. Jünger, X. Cheng, I. Ott, S. Wölfl, *Metallomics*, **2014**, *6*, 1591–1601.

[60] F. Guidi, M. Puglia, C. Gabbiani, I. Landini, T. Gamberi, D. Fregona, M. A. Cinellu, S. Nobili, E. Mini, L. Bini, P. A. Modesti, A. Modesti, L. Messori, *Mol. BioSyst*., **2012**, *8*, 985–993.

[61] A. D. Smith, V. C. Morris, O. A. Levander, *Int. J. Vitam. Nutr. Res.* **2001**, *71* (1), 87–92.

[62] R. Auerbach, Models for angiogenesis. In *Angiogenesis*; Figg, W., Folkman, J., Eds.; Springer US, **2008**, pp 299–312.

Entry for the Table of Contents

FULL PAPER

Iron to Gold: The ferrocenyl substitution of gold(I) NHC complexes augmented their interference with tumor cell redox homeostasis, and their antivascular effects. The complex shown was well tolerated by mice and highly efficacious against invasive B16-F10 melanoma xenograft tumors

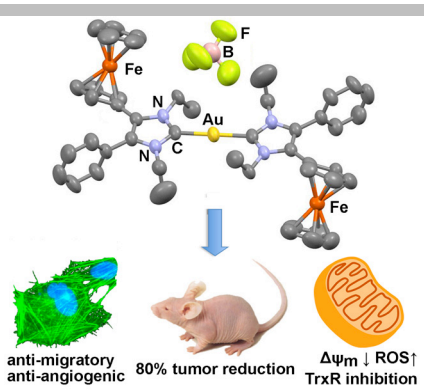

*Julienne K. Muenzner, Bernhard Biersack, Alexander Albrecht, Tobias Rehm, Ulrike Lacher, Wolfgang Milius, Angela Casini, Jing-Jing Zhang, Ingo Ott, Viktor Brabec, Olga Stuchlikova, Ion C. Andronache, Leonard Kaps, Detlef Schuppan, and Rainer Schobert**

Page No. – Page No.

Ferrocenyl-Coupled N-Heterocyclic Carbene Complexes of Gold(I): a Successful Approach to Multinuclear Anticancer Drugs